A vortex force analysis of the interaction of rip currents and surface gravity waves

B. Weir,[1] Y. Uchiyama,[2] E. M. Lane,[3] J. M. Restrepo,[1] and J. C. McWilliams[2]

Received 8 March 2010; revised 20 December 2010; accepted 7 January 2011; published 3 May 2011.

[1] We use the vortex force formalism to analyze the effect of rip currents on their own wave forcing. The vortex force formalism allows us to decompose the wave forcing into the nonconservative flux of momentum due to wave breaking and the conservative vortex force. Following Yu and Slinn (2003), we consider rip currents initially generated by alongshore variation of wave breaking due to a perturbation of a barred bottom topography. This variation is reduced in magnitude by two current effects on waves: wave ray bending and the flux of wave energy by currents. We compute the change in wave energy caused by these two effects on their own and use this to show that their relative magnitude scales with the square of the ratio of the length to width of the rip current. Both effects increase the wave height over the channels of the longshore bar, which leads to more wave breaking and counterbalances its longshore variation due to bottom refraction. In comparison to wave breaking, the change in the vortex force is negligible. Next, we show how the reduction in wave breaking is similar to an enhanced bottom friction. We then analyze the dependence of this relationship on the breaking parameterization, angle of incidence of the waves, and bottom drag law.

Citation: Weir, B., Y. Uchiyama, E. M. Lane, J. M. Restrepo, and J. C. McWilliams (2011), A vortex force analysis of the interaction of rip currents and surface gravity waves, *J. Geophys. Res.*, *116*, C05001, doi:10.1029/2010JC006232.

1. Introduction

[2] Rip currents are strong, seaward flows formed by longshore variation of the wave-induced momentum flux. They are responsible for the recirculation of water accumulated on a beach by a weaker and broader shoreward flow. Rip currents were first recognized as an object of scientific interest by *Shepard* [1936]. Their field observation dates back to *Shepard et al.* [1941], *Shepard and Inman* [1950], and *McKenzie* [1958], who noted that rip currents were largely a surface phenomena fed by convergence of the longshore current, and that they usually fluctuate in time, complicating the collection of detailed observational evidence.

[3] There are a number of possible physical scenarios accounting for the existence and regular spacing of rip currents. The first is due to *Bowen* [1969] and *Bowen and Inman* [1969], who attributed rip currents to the interaction of incoming swell with standing edge waves. However, in the absence of headlands there is no clear explanation for the presence of standing edge waves. Rip currents may also arise as a hydrodynamical instability caused by the refraction of waves by currents. Investigation of this generation mechanism began with *LeBlond and Tang* [1974] and was expanded upon by *Dalrymple and Lozano* [1978], *Falqués et al.* [1999], *Yu* [2006], and *Hasan et al.* [2009]. In this paper we consider longshore variation of the wave-induced momentum flux due to refraction by a barred bottom topography with an imposed longshore perturbation [*Sonu*, 1972; *Noda*, 1974].

[4] The effect of wave-current interaction on model predictions of rip currents dates back to the work of *LeBlond and Tang* [1974], who noted that the flux of wave energy by currents decreases/increases the wave energy over the peaks/channels of the longshore bar. This reduces the longshore variation of wave breaking, and hence the strength of the rip currents. *Yu and Slinn* [2003, hereafter YS03] showed that wave ray bending has a comparable, if not stronger, effect on the wave energy, and that the combined effect of both current effects on waves (CEW) qualitatively changes the steady state and instability mechanism of rip currents. When CEW are neglected, the instability is a result of the lengthening of the rip currents due to advection. Far to sea, the depth is large and the dissipation due to bottom friction is low. The unstable oscillations of these rips are similar to those of a Bickley jet [*Haller and Dalrymple*, 2001]. When CEW are included the flux of momentum from waves to currents due to wave breaking decreases significantly, which impedes the seaward growth of the rips. The instability of these currents usually features the ejection of vorticity generated in the longshore trough, but can have many forms [*Kennedy and Zhang*, 2008]. The above is detailed in greater generality by *Haas et al.* [2003], whose numerical and experimental results include the effect of depth variation as well.

[1]Department of Mathematics, University of Arizona, Tucson, Arizona, USA.
[2]Institute of Geophysics and Planetary Physics, University of California, Los Angeles, California, USA.
[3]Hydrodynamics Group, National Institute for Water and Atmospheric Research, Christchurch, New Zealand.

0148-0227/11/2010JC006232

[5] The wave-induced momentum flux is commonly described using the radiation stress (RS) first developed by *Longuet-Higgins and Stewart* [1960, 1961, 1962, 1964] and given a general derivation by *Hasselmann* [1971]. In this paper we use the vortex force (VF) formalism first developed by *Craik and Leibovich* [1976]. *McWilliams et al.* [2004] used the VF formalism to develop a complete description of the conservative dynamics of waves and currents. The relationship between the RS and VF was established by *Lane et al.* [2007], who demonstrated how these two formalisms are compatible for the wave-current interaction problem at large spatiotemporal scales. The VF formalism is particularly attractive because it decouples the conservative wave effects on currents (WEC) as a vortex force and a Bernoulli head.

[6] A primary goal of this paper is to apply the VF formalism to the dynamics of rip currents and show that even for this complex flow, the description of the WEC is relatively simple. The comparison of the VF and RS formalisms has potential implications to modeling more complex flows. Our analysis also complements the work of YS03 with three new geophysical insights. First, that the effect of wave ray bending on the wave energy relative to the flux of wave energy by the current velocity scales as the square of the ratio of the length to width of the rip. Next, that the feedback loop on the currents due to CEW is similar to an enhanced bottom friction. Finally, that when the swell is narrow banded, it is sufficient to consider wave breaking parameterizations that are power laws, and that as the exponent increases, so does the strength of the enhanced bottom friction.

[7] In section 2 we present the basic rip current problem, which includes defining the bottom topography we use for all numerical experiments, the model equations, and the two model types: one which includes CEW and the other which does not. In section 3 we apply the VF formalism to the analysis of the CEW. This includes an explanation of how increasing the angle of incidence of the waves decreases the magnitude of the CEW, and an analysis of the dependence of our results on the choice of wave breaking parameterization and bottom drag law. In the appendix we demonstrate the equivalence of the VF and RS analysis of rip currents. This reinforces the similar findings of *Lane et al.* [2007] for a case with nonconservative forces on the waves and currents.

2. The Model Equations

[8] We consider a rectangular basin and a bottom topography that is constant over all time. The waves, which approach the shore from far out to sea at a given angle, are assumed to have small wave steepness and a spectrum with a single peak. We assume that the waves are well described by a monochromatic wave with the root-mean-square wave height and frequency corresponding to the spectral peak. We use the ray equations [*Mei*, 1989] for the waves, and the equations for the Eulerian current $\mathbf{u}$ follow from those governing the total flow by averaging over several wave periods as by *McWilliams et al.* [2004]. We neglect the Coriolis force. Though potentially important, we ignore wave set up and set down effects, and suppose that the pressure P is in hydrostatic balance so that $P = \rho g(\zeta - z)$, where ζ is the (constant) mean sea elevation, g is the constant of gravity, and, for simplicity, the water has a constant density $\rho = 1000$ kg m^{-3}. The rip currents are driven by the flux of momentum from the waves due to wave breaking and dissipated by bottom drag.

[9] In order to analyze the CEW, we consider two wave-current interaction models based on those by *Uchiyama et al.* [2009]: (1) WEC+CEW, which includes CEW, and (2) WEC-only, which does not. In both models, we first allow the waves to reach a steady state without CEW. For the WEC-only model, the WEC are held constant in time at this state, whereas for the WEC+CEW model the WEC evolve in time, dynamically forcing the currents. The surface gravity wave equations are presented for the WEC+CEW interaction model only, with the understanding that the WEC-only equations are the same with the terms involving the current velocity $\mathbf{u}$ omitted.

[10] The horizontal coordinates of the fluid domain are (x, y), where x is aligned with the cross-shore direction, and y the longshore. The vertical coordinate z is aligned opposite to the direction of gravity. We use an east coast configuration so that increasing x corresponds to increasing distance from the shore. The domain is 768 m by 768 m and assumed to be periodic in the alongshore direction. We assume that the nearshore boundary is reflectionless, and there is no net outflow at the offshore boundary. All vectors are horizontal and independent of the depth. For a given vector $\mathbf{v} = (v_1, v_2)$, we denote the vector equal in magnitude and 90° counterclockwise as $\mathbf{v}^{\perp} = (-v_2, v_1)$. We use this definition with the gradient vector ∇ as well, so that

$$\nabla^{\perp} \cdot \mathbf{v} = \frac{\partial v_2}{\partial x} - \frac{\partial v_1}{\partial y} \tag{1}$$

is the vertical component of the curl of $\mathbf{v}$.

[11] The bottom topography depends on the cross-shore coordinate x as

$$\begin{aligned} h_0(x) = &-1.5 \exp\left[-\frac{5}{d_b^2}(x - x_s - d_b)^2\right] \\ &+ 1.35\{1 + \tanh[0.0253(x - x_s)]\} \\ &+ 0.0032\left\{x + \frac{1}{\alpha}\log\left[\frac{\cosh(\alpha(x - x_s))}{\cosh(\alpha x_s)}\right]\right\}, \end{aligned}$$

(see Figure 1a). This topography is based on that used by *Lippmann et al.* [1999] for the 11 October 1990 DELILAH field experiments at Duck, North Carolina. The logarithmic term is introduced to eliminate any difficulties with the depth approaching zero, and its steepness is determined by the parameter $\alpha = 0.02$ m^{-1}. The inner surf zone is defined as the region shoreward of $x_s = 150$ m, so that $d_b = 80$ m is the distance from this zone to the bar. For $x < x_s$, we artificially increase the numerical viscosity, representing the situation when dissipation dominates all other forces. We impose longshore variation of wave breaking by adding the perturbation

$$p(x, y) = \varepsilon \cos\left(\frac{2\pi}{\lambda} y\right) \exp\left[-\frac{5}{d_b^2}(x - x_s - d_b)^2\right], \tag{2}$$

so that $h = (1 + p)h_0$ (see Figure 1b). The parameter λ is the wavelength of the perturbation, and unless specified

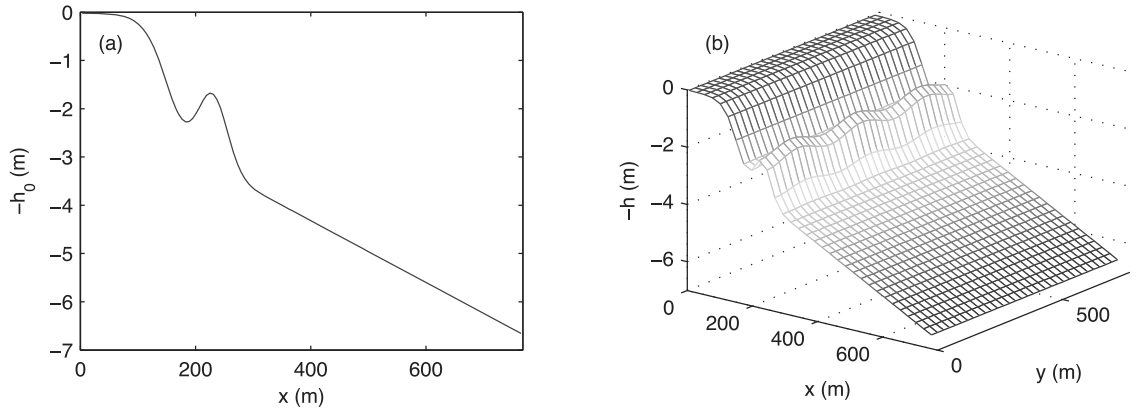

Figure 1. (a) The alongshore mean and (b) the three-dimensional view of the bottom topography. The bar has a longshore perturbation whose magnitude is $\varepsilon = 0.1$ and wavelength is $\lambda = 256$ m.

otherwise we use $\lambda = 256$ m. We refer to the minima of the longshore bar as channels and the maxima as peaks.

2.1. The Surface Gravity Waves

[12] The wave number $\mathbf{k} = (k_1, k_2)$ is the gradient of the wave phase, and is irrotational. The equation for conservation of wave crests is

$$\frac{\partial \mathbf{k}}{\partial t} + \nabla(\mathbf{u}\cdot\mathbf{k} + \sigma) = 0, \tag{3}$$

where the frequency σ satisfies the dispersion relation

$$\sigma^2 = gk\tanh kh \tag{4}$$

and $k = |\mathbf{k}|$ is the modulus of the wave number.

[13] The wave action $\mathcal{A}$ is related to the wave energy E and amplitude A by the identities

$$\mathcal{A} = \frac{E}{\sigma} = \frac{1}{2\sigma}\rho g A^2.$$

In the absence of wave breaking it is a conserved quantity advected by the absolute group velocity $\mathbf{c_g} = \mathbf{u} + \mathbf{C_g}$, where the intrinsic group velocity is

$$\mathbf{C_g} = \frac{\sigma}{2k}\left(1 + \frac{2kh}{\sinh 2kh}\right)\frac{\mathbf{k}}{k}.$$

We include dissipation due to shoaling-induced wave breaking using the theory of periodic bores first suggested by *LeMehaute* [1962], so that the wave action satisfies

$$\frac{\partial \mathcal{A}}{\partial t} + \nabla\cdot\left(\mathbf{c_g}\mathcal{A}\right) = -\frac{\varepsilon_b}{\sigma}. \tag{5}$$

Unless otherwise specified, we use the semiempirical parameterization of *Thornton and Guza* [1983], which we refer to as TG83a,

$$\varepsilon_b = \frac{3\sqrt{\pi}}{16}\rho g f_p B r^3 \frac{H_{\mathrm{rms}}^7}{\gamma^4 h^5},$$

where f_p is the peak frequency of the waves, H_{rms} the root-mean-square wave height such that

$$f_p = \frac{\sigma}{2\pi} \qquad \text{and} \qquad H_{\mathrm{rms}} = 2A$$

and Br and γ are model parameters fit to the data. The parameter Br measures the percentage of the wave face that is broken, and γ the saturation of wave energy, such that when $H_{\mathrm{rms}} = \gamma h$ all waves are assumed to be breaking. In section 3.6 we discuss the dependence of model predictions on other choices of ε_b.

[14] In the numerical simulations below, we assume that far out to sea the waves have a height of 1 m and a period of 10 s, and we use the breaking parameters $Br = 1.3$ and $\gamma = 0.38$. In Figure 2 we plot the steady state wave variables for these choices, the WEC-only model, and the longshore uniform bottom topography h_0. The steady state represents a constant wave period, and the balance of the increase in wave height due to shoaling and the decrease due to breaking.

2.2. The Rip Currents

[15] The equations for the Eulerian current $\mathbf{u}$ are

$$\frac{\partial \mathbf{u}}{\partial t} + \mathbf{u}\cdot\nabla\mathbf{u} + g\nabla\zeta = -\chi\left(\mathbf{u}^{\mathrm{St}}\right)^{\perp} + \mathbf{B} - \mathbf{D}, \tag{6}$$

$$\nabla\cdot\left[h\left(\mathbf{u} + \mathbf{u}^{\mathrm{St}}\right)\right] = 0. \tag{7}$$

The depth-averaged Stokes drift, which we refer to simply as the Stokes drift, is the vector field

$$\mathbf{u}^{\mathrm{St}} = \frac{\mathcal{A}\mathbf{k}}{\rho h} = \frac{|A|^2\sigma\mathbf{k}}{2kh\tanh kh}. \tag{8}$$

The term $\chi\,(\mathbf{u}^{\mathrm{St}})^{\perp}$ is the vortex force, where $\chi = \nabla^{\perp}\cdot\mathbf{u}$ is the (vertical) vorticity of the current. The vector field

$$\mathbf{B} = \frac{\varepsilon_b}{\rho h\sigma}\mathbf{k} \tag{9}$$

is the flux of momentum from waves to currents due to wave breaking. For the moment, we use the linear bottom drag law

$$\mathbf{D} = \mu_f\frac{\mathbf{u}}{h}.$$

In order to demonstrate the importance of CEW, we pick values of the constant μ_f that are $O(10^{-3})$ m s^{-1}. In section 3.8 we examine the appropriateness of this assumption. Since

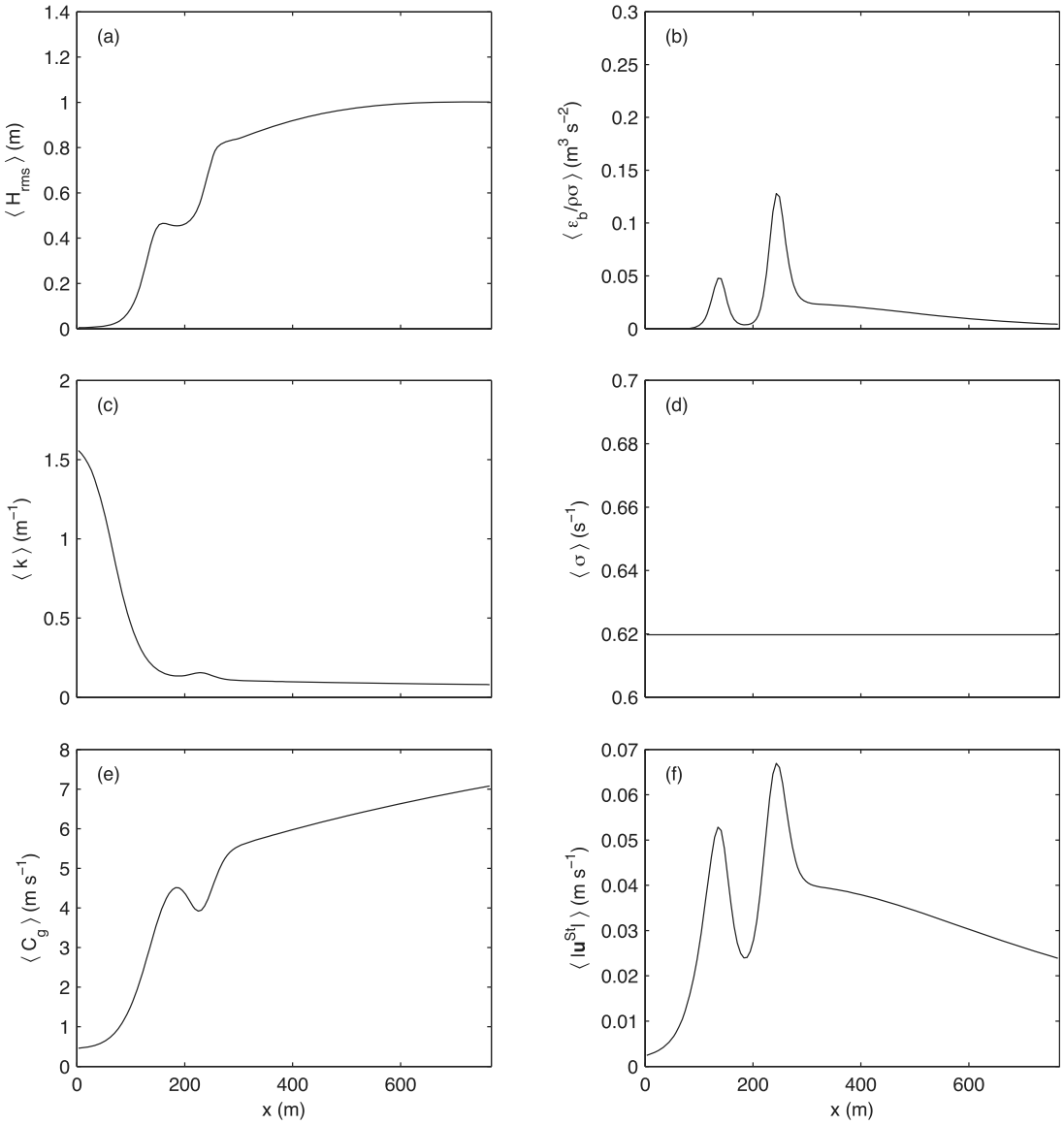

Figure 2. The alongshore means of the steady state wave variables: (a) the root-mean-square wave height, (b) the dissipation of wave action due to breaking, (c) the wave number, (d) the frequency, (e) the magnitude of the group velocity, and (f) the magnitude of the Stokes drift. The alongshore components of the wave number, group velocity, and Stokes drift are negligible compared to the cross-shore components and are not shown.

we make the rigid lid approximation, the pressure force $g\nabla\zeta$ is simply the hydrostatic pressure contribution.

[16] Since the vector field $h(\mathbf{u} + \mathbf{u}^{St})$ is solenoidal, we define a pseudo stream function ψ such that

$$h\left(\mathbf{u} + \mathbf{u}^{St}\right) = \nabla^{\perp}\psi. \tag{10}$$

In terms of the two unknowns ψ and χ, (6) and (7) are equivalent to the two equations

$$\nabla \cdot \left(\frac{1}{h}\nabla\psi\right) = \chi + \nabla^{\perp} \cdot \mathbf{u}^{St}, \tag{11}$$

$$\frac{\partial \chi}{\partial t} + \nabla \cdot \left[\left(\mathbf{u} + \mathbf{u}^{St}\right)\chi\right] = \nabla^{\perp} \cdot (\mathbf{B} - \mathbf{D}). \tag{12}$$

2.3. The Numerical Solution

[17] We compute the wave and current variables as follows. First, we advance (3) and (5) forward in time with no currents until they reach a steady state. Given an initial vorticity field, we solve (11) for the stream function ψ, then (10) for the Lagrangian velocity $\mathbf{u} + \mathbf{u}^{St}$. We compute the vorticity at the next step in time using (12). Finally, for the WEC+CEW model, we advance the waves according to (3) and (5).

[18] We use the corner transport upwind method with the monotonized central difference flux limiter [*LeVeque*, 2002, p. 115]. The corner transport upwind method is second-order accurate in both time and space. The use of a flux limiter reduces the method to a formally first-order accurate method, yet in practice the limited method removes spurious

oscillations and still produces results that are comparable to second-order accurate methods. We use a uniform grid spacing of $\Delta x = \Delta y = 3$ m, and a variable time step Δt for the wave equations (3) and (5) such that the CFL number is always 0.9. As *Haas et al.* [2003] did we update the vorticity equation, which is formally decoupled from the wave equations, after a fixed multiple of the wave time step Δt. For our particular grid spacing any multiple between one and the maximum multiple such that the CFL condition is satisfied give nearly identical results. For finer grid spacings, a multiple such that the current equations are updated every 5 seconds gives accurate results that remain bounded. We note that one advantage of the VF formalism over the RS formalism is numerical: the former requires taking one less derivative in space, and is thus less susceptible to numerical oscillations.

3. Analysis of Rip Current Effects on Waves

[19] The analysis in this section applies to any bottom topography with the same qualitative properties as our choice, i.e., monotonically increasing depth from the edge inner surf zone to the far sea, except at a longshore bar, and variation in the longshore direction that is small compared to that in the cross-shore direction. These assumptions are necessary so that the resulting currents are rips. Our analysis requires as well that the wave steepness Ak and the strength of the currents compared to the group velocity of the waves are always negligible. We assume that these quantities are the same or lower order as the longshore variation of the bottom topography, so that $Ak = O(\varepsilon)$ and $|\mathbf{u}/\mathbf{C_g}| = O(\varepsilon)$.

[20] We further restrict our attention to waves whose angle of incidence is near normal. We may then assume

$$\delta = \frac{k_2}{k_1} = \tan\theta \ll 1,$$

where θ is the angle of incidence of the waves far to sea. Throughout, we will avoid carrying out the formal nondimensionalization and scaling of quantities, with the understanding that when we make approximations, it is the ratio of the two terms in this approximation that have the specified dimensionless order. To begin, the near-normal assumption implies

$$k = \sqrt{k_1^2 + k_2^2} = -k_1 + O(\delta^2).$$

For a given value of ε, we consider all values of δ ranging from 0 up to ε. When $\varepsilon = 0.1$, this corresponds to angles of incidence θ between 0° and about 6°. This ensures that the alongshore means of the *current* variables are small compared to their alongshore fluctuations, i.e., that the current is dominated by a rip current flow and not a longshore flow. The *wave* variables, on the other hand, are predominantly the values of their longshore means, ε being a measure of their deviation away from these means.

[21] In Figure 3 we show the vorticity fields of the WEC-only (Figure 3a) and the WEC+CEW (Figure 3b) models for a bottom friction of $\mu_f = 0.002$ m s^{-1} at $t = 80$ min. This is a reproduction of Figure 2 of YS03 for the TG83a wave breaking model. The most striking effect of the inclusion of CEW is the shortening of the rip currents. This occurs because the CEW diminish the flux of momentum from the waves to the currents due to wave breaking, which is the term $\nabla^\perp \cdot \mathbf{B}$ in the vorticity equation (12) (see Figure 4, which is a reproduction of Figure 4c and 4c of YS03).

3.1. Longshore Means and Fluctuations

[22] For a function f of the horizontal coordinates, we define the alongshore mean and fluctuation as

$$\langle f \rangle = \frac{1}{L}\int_0^L f(x,y)\,dy, \quad \text{and} \quad \widetilde{f} = f - \langle f \rangle,$$

where $L = 768$ m is the domain length in the longshore direction. Since the fluctuation of the bottom topography is $O(\varepsilon)$, where ε is the amplitude of the perturbation to the longshore bar, the fluctuation of f is also $O(\varepsilon)$. Hence, up to $O(\varepsilon)$ the alongshore means of the wave variables are the solution to the problem in the cross-shore variable x only, depicted in Figure 2. When δ is nonzero, the irrotationality of the wave number ensures that to $O(\varepsilon)$, the longshore component k_2 of the wave number is an $O(\delta^2)$ constant, as is the angle of incidence.

[23] When currents are weak compared to waves, the currents do not change the longshore means of the wave variables. Nevertheless, they do change the fluctuations of the wave variables. As noted by YS03, this change can be quite substantial, and as a result, cause a noticeable reduction in the magnitude of the WEC. Below, we derive identities for the change in the wave variables due to the currents, then use these identities to analyze the CEW and their dependence on the length and width of the rip, the incoming angle of the waves, the choice of breaking parameterization, and the bottom drag law. We use the shallow water approximation $kh \to 0$ for mathematical convenience, but the assumption is not essential to the results.

[24] Since all longshore fluctuations are $O(\varepsilon)$, they satisfy the approximate product rule

$$\widetilde{fg} \approx \langle f \rangle \widetilde{g} + \widetilde{f}\langle g \rangle.$$

Henceforth, we use $\approx$ to denote equivalence up to the maximum of $O(\varepsilon^2)$, $O(\varepsilon\delta)$, and $O(\delta^2)$. We make the additional definition that for a function f of the *wave* variables, its difference due to CEW is defined as

$$\Delta f = \widetilde{f}^{\text{WEC+CEW}} - \widetilde{f}^{\text{WEC-only}} \approx f^{\text{WEC+CEW}} - f^{\text{WEC-only}},$$

where $f^{\text{WEC-only}}$ is the steady state value of f for the WEC-only interaction model, and likewise for WEC+CEW. The second equality follows since currents are lower order than waves. Hence, Δ also satisfies the same approximate product rule as the longshore fluctuations.

3.2. The Doppler Shift and Wave Ray Bending

[25] We begin our analysis with the changes in the wavefield. From the equation for the wave number (3), we see that for the steady state waves

$$\Delta\sigma = -\Delta(\mathbf{u}\cdot\mathbf{k}) \approx -u\langle k_1 \rangle. \tag{13}$$

This change is the Doppler shift and it is depicted in Figure 5 (when there are no CEW, the steady frequency is the constant $\sigma_0 = 0.62$ s^{-1} everywhere, set at the offshore boundary).

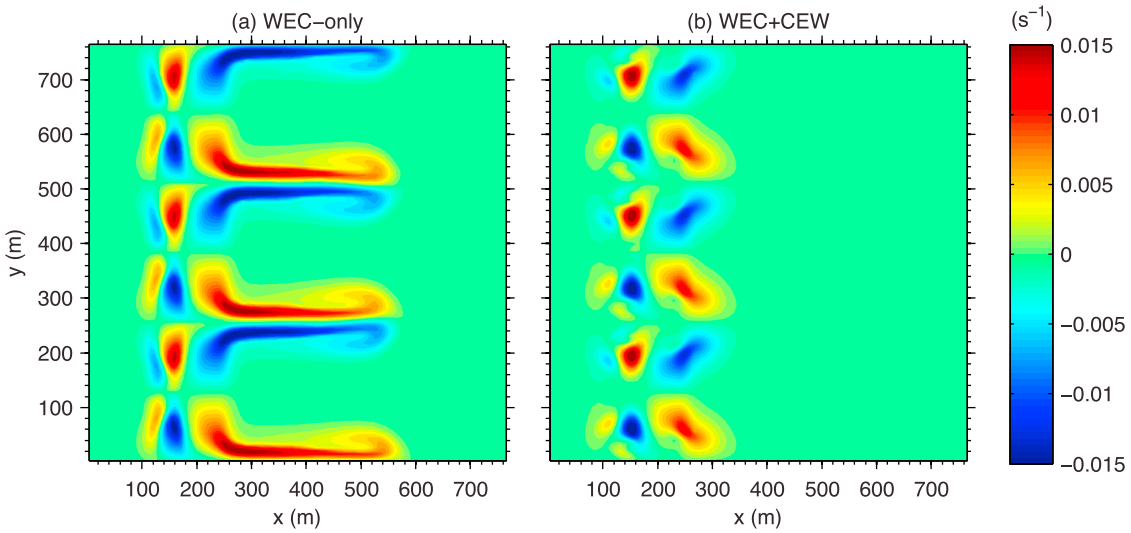

Figure 3. Comparison of the instantaneous vorticity fields for the (a) WEC-only and (b) WEC+CEW models at $t = 80$ min with $\mu_f = 0.002$ m s^{-1}. Notice the considerable difference in the seaward (positive x) extent of the contours from Figure 3a to Figure 3b. The WEC-only current is unstable and oscillates sinusoidally at the rip head, while the WEC+CEW current is stable.

[26] We refer to "wave ray bending" as the changes in the wave number, along with the subsequent changes in the wave energy and breaking. Since $\Delta(\sigma k^{-1}) = \Delta\sqrt{gh} = 0$, we may use the approximate product rule to compute

$$\Delta k_1 \approx -\left\langle \frac{k}{\sigma} \right\rangle \Delta\sigma \approx -\left\langle \frac{\sigma}{gh} \right\rangle u.$$

The equation for Δk_2 then follows from the irrotationality of the wave number **k**. It is

$$\frac{\partial}{\partial x}(\Delta k_2) \approx -\left\langle \frac{\sigma}{gh} \right\rangle \frac{\partial u}{\partial y}. \tag{14}$$

If $\Delta\sigma$ is alongshore uniform, then $\Delta k_2 \equiv 0$. Hence, alongshore variation of the Doppler shift is the cause of wave ray bending. Equation (14) is an ordinary differential equation parameterized by the alongshore variable y, such that $\Delta k_2 = 0$ at $x = L$, the offshore boundary. Its solution is

$$\Delta k_2 = \int_x^L \left\langle \frac{\sigma}{gh} \right\rangle \frac{\partial u}{\partial y} dx'. \tag{15}$$

[27] The resulting change in the longshore component of the group velocity is

$$\begin{aligned} \Delta C_{g_2} &\approx \left\langle \frac{gh}{\sigma} \right\rangle \Delta k_2, \\ &= \left\langle \frac{gh}{\sigma} \right\rangle \int_x^L \left\langle \frac{\sigma}{gh} \right\rangle \frac{\partial u}{\partial y} dx', \end{aligned} \tag{16}$$

whereas the cross-shore component of the group velocity is left unchanged by CEW, since $C_{g_1} \approx -C_g = -\sqrt{gh}$. When there are no CEW, refraction by the bottom topography

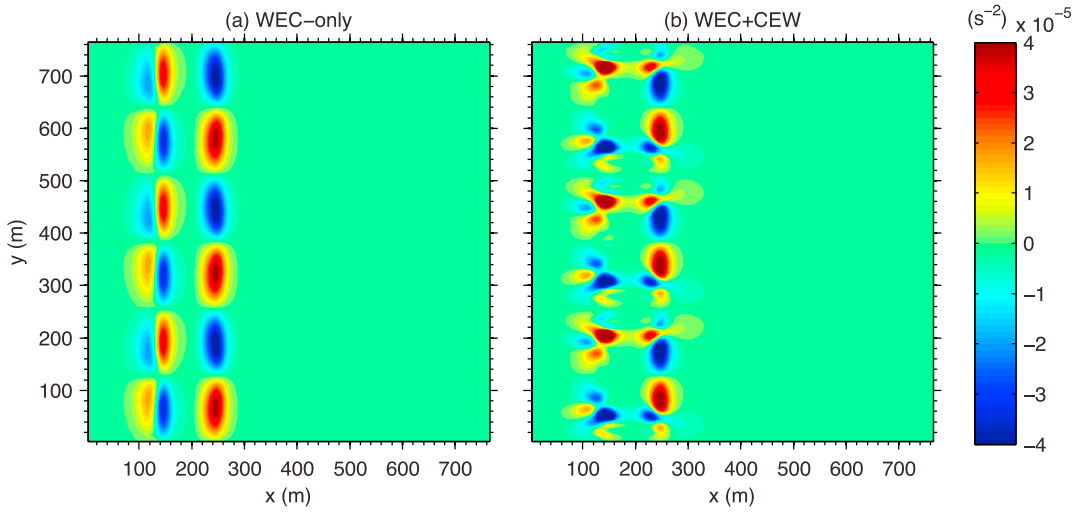

Figure 4. Comparison of the forcing due to wave breaking on current vorticity $\nabla^{\perp} \cdot \mathbf{B}$ for the (a) WEC-only and (b) WEC+CEW models.

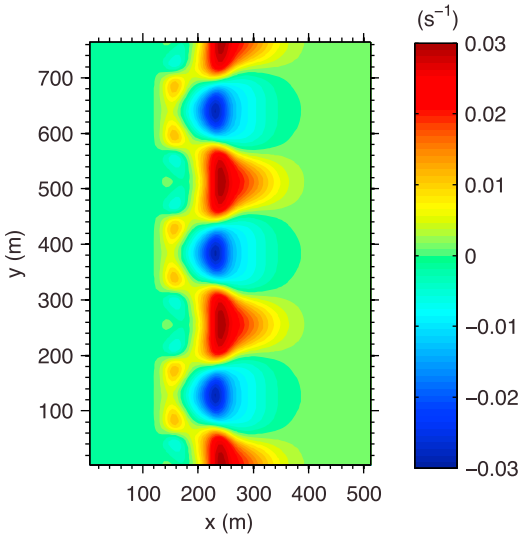

Figure 5. The Doppler shift $\Delta\sigma$. For the WEC-only model, σ is the constant $\sigma_0 = 0.62$ s^{-1}.

forces the wave rays to diverge away from the rip channels toward the peaks of the bar (Figure 6a). When there are CEW, the longshore component of the group velocity changes sign, and the wave rays now diverge from the peaks of the bar and converge toward the rip channels (Figure 6b).

3.3. Current Effects on Wave Height

[28] In order to analyze the change in wave height, we first find the change in wave energy ΔE, then use the relation

$$\Delta H_{\mathrm{rms}} = \frac{4}{\rho g \langle H_{\mathrm{rms}} \rangle} \Delta E,$$

which follows from the identity $\rho g H_{\mathrm{rms}}^2 = 8E$. Applying the operator Δ to both sides of (5) shows that

$$\frac{\partial}{\partial x}\left(\langle C_{g_1} \rangle \Delta E\right) + \frac{7}{2}\left\langle \frac{\varepsilon_b}{E} \right\rangle \Delta E = -\frac{\partial}{\partial y}\left(\Delta C_{g_2}\right)\langle E \rangle - \nabla \cdot [(2u, v)\langle E \rangle]. \tag{17}$$

The factor of two in front of the cross-shore current u is due to the Doppler shift, which reinforces the effect of the cross-shore current.

[29] Since ΔE is a linear function of the two terms on the right-hand side of (17), we decompose it as

$$\Delta E = \Delta_{\mathrm{WRB}} E + \Delta_{\mathrm{CF}} E,$$

where $\Delta_{\mathrm{WRB}} E$ is the effect of the first term (wave ray bending) and $\Delta_{\mathrm{CF}} E$ the effect of the second, which we refer to as the current flux of wave energy. We solve for these two terms using an integrating factor $M = M(x)$ such that

$$\Delta_{\mathrm{WRB}} E = \frac{1}{M\langle C_{g_1} \rangle} \int_x^L M \frac{\partial}{\partial y}\left(\Delta C_{g_2}\right)\langle E \rangle \, dx' \tag{18}$$

$$\Delta_{\mathrm{CF}} E = \frac{1}{M\langle C_{g_1} \rangle} \int_x^L M \nabla \cdot [(2u, v)\langle E \rangle] \, dx', \tag{19}$$

$$M(x) = \exp\left(\int_x^L \frac{7}{2}\left\langle \frac{\varepsilon_b}{E} \right\rangle dx' \right). \tag{20}$$

We define $\Delta_{\mathrm{WRB}} H_{\mathrm{rms}}$ and $\Delta_{\mathrm{CF}} H_{\mathrm{rms}}$ as the corresponding changes in the wave height.

[30] Since wave ray bending causes wave rays to concentrate over rip channels, rather than the peaks in the longshore bar, it forces wave energy from the peaks toward the channels. In our numerical solutions, the effect of wave ray bending on the wave energy (Figure 7a) is approximately two and a half times stronger than that of the current flux alone (Figure 7b). If l is a typical length scale of the rip currents and w is a typical width, then using (16) in (18) and dividing by (19) we see that the ratio $\Delta_{\mathrm{WRB}} E / \Delta_{\mathrm{CF}} E$ scales as $(l/w)^2$.

3.4. The Stokes Drift and Vortex Force

[31] Apart from the wave breaking momentum flux, the only other WEC we consider is the vortex force. Up to $O(\varepsilon^2)$, the term representing the vortex force in the vorticity equation (12) is

$$\nabla \cdot \left(\mathbf{u}^{\mathrm{St}} \chi\right) \approx \frac{\partial}{\partial x}\left(\langle u^{\mathrm{St}} \rangle \chi\right). \tag{21}$$

Since the waves are directed onshore, the mean Stokes drift $\langle u^{\mathrm{St}} \rangle$ is negative everywhere. The vortex force thus opposes the seaward advection of vorticity by the Eulerian current. Furthermore, the current effect on $\langle u^{\mathrm{St}} \rangle$ is $O(\varepsilon)$. Thus, any change in the vortex force at leading order is due entirely to the change in the steady current vorticity χ, and if the wave breaking momentum flux does not change, the vortex force remains unchanged as well. In Figure 8 we decompose the Lagrangian flux of vorticity $\nabla^{\perp} \cdot (\mathbf{u} + \mathbf{u}^{\mathrm{St}})$ in equation (12) for both the WEC-only and WEC+CEW models. Even though changes in $\nabla^{\perp} \cdot \mathbf{B}$ modify the steady vorticity field, the changes in the vortex force from Figures 8a–8d are

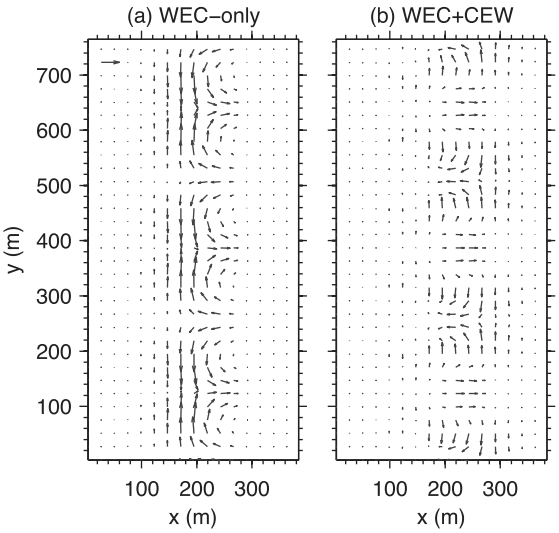

Figure 6. Comparison of the alongshore fluctuations of the steady group velocity, $\widetilde{\mathbf{C}_{\mathbf{g}}}$ for the (a) WEC-only and (b) WEC+CEW models. The sign of the alongshore component $\widetilde{C_{g_2}}$ determines whether the wave rays diverge (Figure 6a) or converge (Figure 6b) over the rip channels. The reference arrow in the top left corner of Figure 6a is for $|\widetilde{\mathbf{C}_{\mathbf{g}}}| = 0.33$ m s^{-1}.

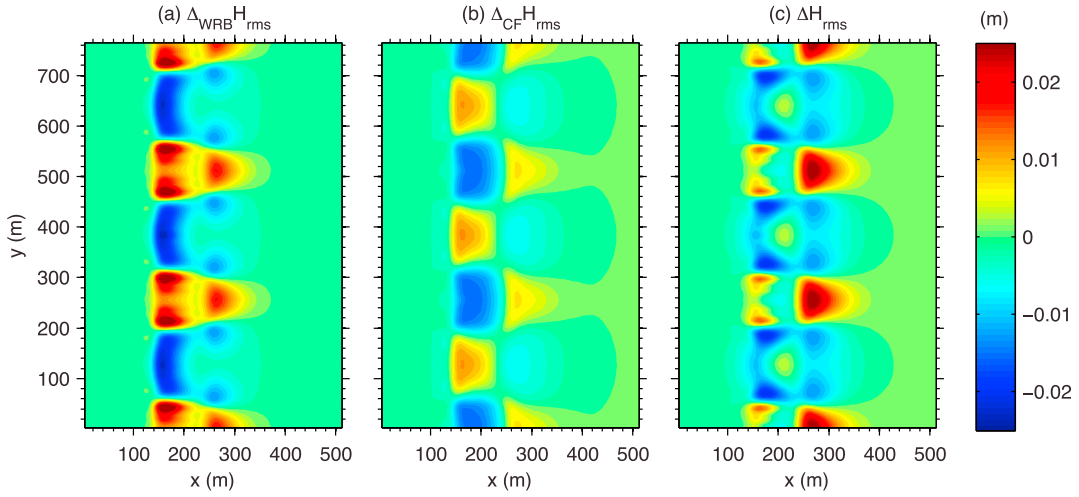

Figure 7. Change in wave height due to CEW: (a) change due to wave ray bending, (b) change due to flux by the current velocity, and (c) total change.

minimal, the dominant change being in the flux of vorticity by the Eulerian current from Figure 8c to frame Figure 8d.

3.5. The Wave Breaking Momentum Flux

[32] Applying the operator Δ to (9) and using the TG83a model parameterization, we may decompose the change in wave breaking momentum flux as

$$\Delta\left(\nabla^{\perp}\cdot\mathbf{B}\right)\approx\left\{7\left\langle\frac{\varepsilon_b}{\rho h\sigma}\right\rangle\left\langle\frac{k}{H_{\rm rms}}\right\rangle\right\}\frac{\partial}{\partial y}(\Delta H_{\rm rms})+\left\{\frac{\partial}{\partial x}\left\langle\frac{\varepsilon_b}{\rho h\sigma}\right\rangle\right\}\Delta k_2. \tag{22}$$

Recall that $\mathbf{k}$ is irrotational, so $\nabla^{\perp}\cdot\mathbf{k}=0$. Thus, knowing the changes in the wave number and the wave height allows us to completely determine the change in the generation of vorticity due to wave breaking.

[33] Now suppose that within the rip

$$v\ll u,\qquad \frac{\partial}{\partial x}\ll\frac{\partial}{\partial y}.$$

The second assumption being equivalent to $w\ll l$, where w is a typical width and l a typical length of the rip (see *Haller and Dalrymple* [2001] for a more systematic treatment of WEC-only currents given these assumptions). Then we may use (15) to write

$$\Delta k_2\approx-\int_x^L\left\langle\frac{\sigma}{gh}\right\rangle\omega\,dx'.$$

Since the ratio of the rip current width to length is negligible compared to 1, the change in wave energy is due entirely to wave ray bending. Hence,

$$\Delta H_{\rm rms}=-\frac{4}{\rho g\langle C_{g_1}\rangle H_{\rm rms}M}\int_x^L M\langle h\rangle\left(\int_{x'}^L\left\langle\frac{1}{h}\right\rangle\frac{\partial\omega}{\partial y}\,dx''\right)dx'.$$

Substituting these expressions into (22), we may thus express the WEC+CEW model for the vorticity as the WEC-only model plus an extra forcing that is an integral operator of the vorticity. In general, it is no easier to solve this equation than the full WEC+CEW model. Instead, we assume that the rip is self similar in such a way that we may express the change in wave breaking momentum flux in terms of the bottom friction (Figure 9).

[34] In order to find the best expression for $\Delta\left(\nabla^{\perp}\cdot\mathbf{B}\right)$ in terms of a linear friction, we form the functional

$$J(\mu)=\left\{\int_0^L\int_{200}^L\left[\Delta\left(\nabla^{\perp}\cdot\mathbf{B}\right)-\mu\left(\nabla^{\perp}\cdot\frac{\mathbf{u}}{h}\right)\right]^p dx\,dy\right\}^{1/p}$$

and minimize to find $\mu_{\rm CEW}$. We chose the region shoreward of $x=200$ m in order to concentrate the minimization on the region occupied by the rip. If $p=2$, then J measures the root-mean-square difference. We pick $p=8$ based on the best visual fit of the WEC+CEW model with the linear bottom friction coefficient μ_f and the WEC-only model using the enhanced bottom friction $\mu_{\rm enh}=\mu_f+\mu_{\rm CEW}$.

[35] The comparison of the WEC+CEW rip with $\mu_f=0.002$ m s^{-1} and the WEC-only rip with $\mu_{\rm enh}=0.0065$ m s^{-1} is depicted in Figure 10 and the minima of the functional J is depicted for a range of bottom frictions in Figure 11. Notice that even when $\mu_f=0$, the enhanced bottom friction is greater than 0.005 m s^{-1}, a value in the stable regime for the WEC-only model.

3.6. Wave Breaking Parameterizations

[36] Many wave breaking parameterizations including those proposed by *Thornton and Guza* [1983], *Church and Thornton* [1993], and *Roelvink* [1993] have the form

$$\frac{\varepsilon_b}{\rho h\sigma}=C_B h f_B(S), \tag{23}$$

where C_B is a constant and

$$S=\frac{H_{\rm rms}}{\gamma h}$$

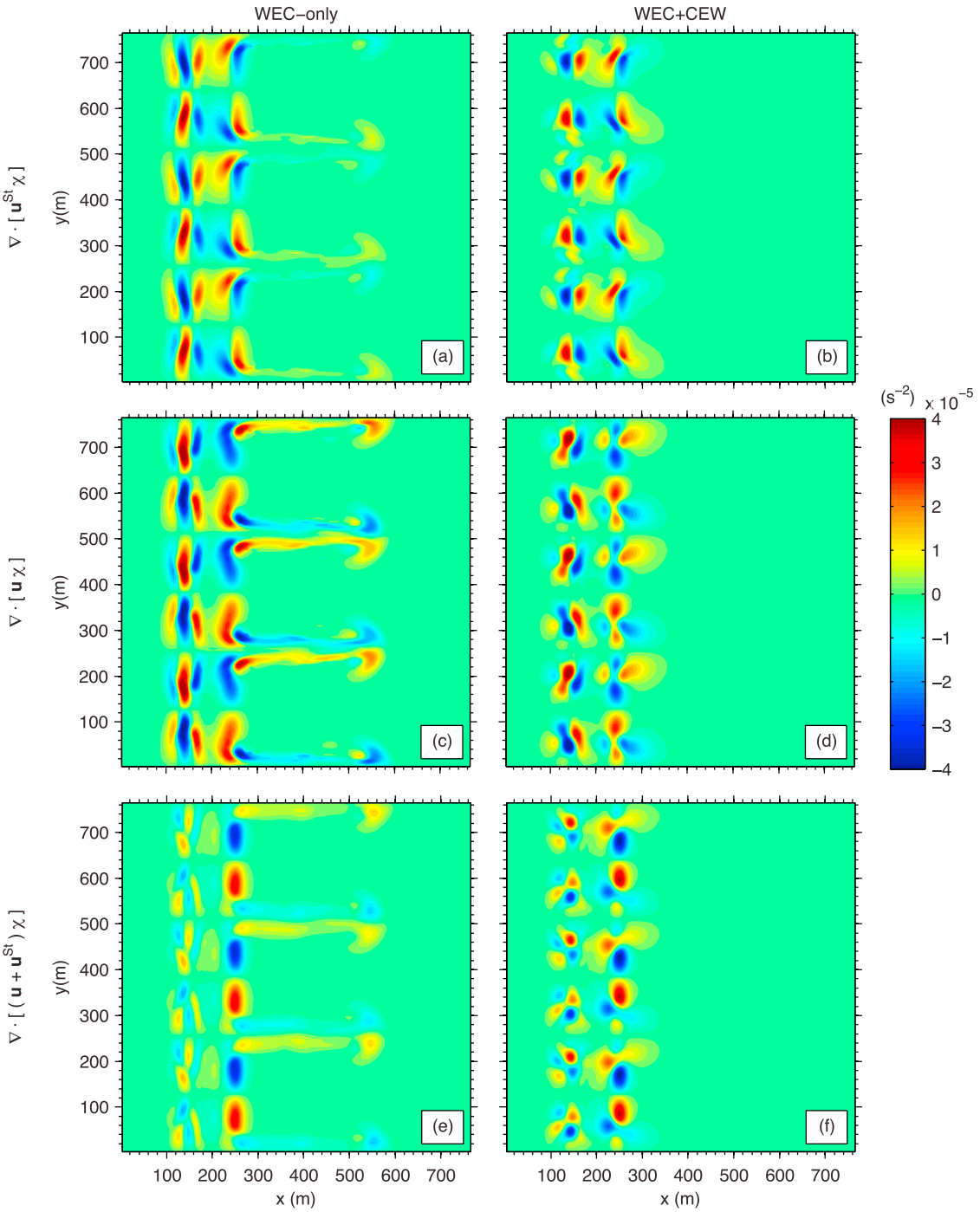

Figure 8. Component by component decomposition of the advection of vorticity, for the (a, c, e) WEC-only and (b, d, f) WEC+CEW model type.

is the coefficient of wave energy saturation, such that when $S = 1$ all waves are assumed to be breaking. Recall that we previously defined ε_b in the TG83a model. For this definition,

$$C_B = \frac{3}{32\sqrt{\pi}} gBr^3\gamma^3, \qquad f_B(S) = S^7.$$

[37] We now consider two alternative wave breaking parameterizations. The first, the TG83b model,

$$\varepsilon_b = \frac{3\sqrt{\pi}}{16}\rho g f_p B r^3 \frac{H_{\mathrm{rms}}^5}{\gamma^2 h^3}\left[1 - \frac{1}{\left(1 + (H_{\mathrm{rms}}/\gamma h)^2\right)^{5/2}}\right],$$

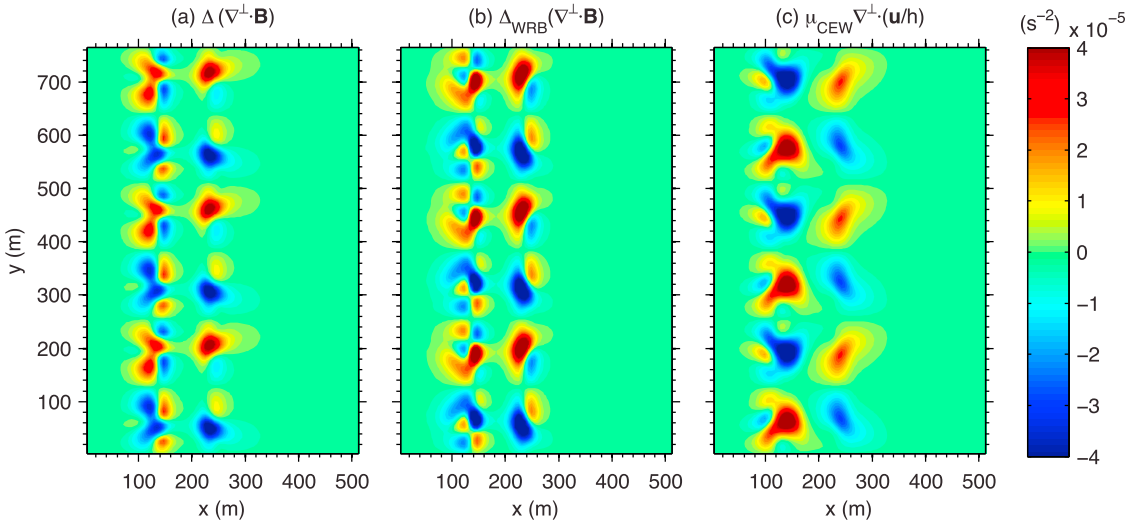

Figure 9. Comparison of (a) the total in change $\nabla^{\perp} \cdot \mathbf{B}$, (b) the change with the current flux of wave energy neglected, and (c) a rescaled linear friction term, where $\mu_{\mathrm{CEW}} = 0.0045$ m s^{-1}. In particular, compare the frames in the region shoreward of $x = 200$ m.

is also proposed by *Thornton and Guza* [1983]. As a further refinement to TG83b, *Church and Thornton* [1993] use the CT93 model,

$$\varepsilon_b = \frac{3\sqrt{\pi}}{16}\rho g f_p B r^3 \frac{H_{\mathrm{rms}}^3}{h} N \left[1 - \frac{1}{\left(1 + (H_{\mathrm{rms}}/\gamma h)^2\right)^{5/2}}\right],$$

where

$$N = 1 + \tanh\left[8\left(\frac{H_{\mathrm{rms}}}{\gamma h} - 1\right)\right].$$

[38] In Figure 12, we plot the function f_B, defined in (23), for each of these three choices of wave breaking parameterization: the TG83a, TG83b, and CT93 models. To facilitate the comparison, we normalize the function f_B so that $f_B(1) = 1$ for all three parameterizations. This is equivalent to using a parameter Br for the TG83a model that is 0.94 times the value used for the TG83b and CT93 models. Each of the functions f_B in Figure 12 are well approximated by a power law (the TG83a model is a power law). For comparison with the TG83b and CT93 models, we plot $f_B(S) = S^6$ and $f_B(S) = S^{14}$. Not pictured, is the class of wave breaking parameterizations derived by *Roelvink* [1993]

$$\varepsilon_b = \frac{1}{4}\rho g f_p B r^3 \frac{H_{\mathrm{rms}}^3}{h}\left(\frac{H_{\mathrm{rms}}}{\gamma h}\right)^m \left\{1 - \exp\left[-\left(\frac{H_{\mathrm{rms}}}{\gamma h}\right)^n\right]\right\},$$

where m and n are arbitrary nonnegative numbers. In general, for $0 \le S \le 1$, it is sufficient to make the approximation

$$1 - \exp[-S^n] \approx \left(1 - e^{-1}\right)S^n,$$

corresponding to the first term in the Taylor series of the left-hand side. We thus treat these parameterizations as power laws, so that $f_B(S) = S^a$, and analyze the dependence of our results on the parameter a.

[39] The three parameterizations can be ordered from largest to smallest values the exponent a as CT93, TG83a, and TG83b. Since its exponent is the largest, runs using the CT93 model allow more shoaling of the incoming wave before breaking occurs than the TG83 models (Figure 13a). When breaking does occur for the CT93 model, it is more intense (Figure 13b) than for the other models. This can lead to scenarios where the CT93 currents are unstable, yet the TG83 currents are stable.

[40] In particular, notice that the first term on the right-hand side of (22) is multiplied by a factor of the exponent a (in this case $a = 7$). Hence, as the exponent of a increases, so does the strength of the current effect on the wave breaking momentum flux, as does the value of μ_{CEW}.

3.7. Angle of Incidence

[41] Figure 14 depicts $\nabla^{\perp} \cdot \widetilde{\mathbf{B}}$ for incoming angles of 1° (a), 3° (b), and 6° (c). We ignore the alongshore mean $\nabla^{\perp} \cdot \langle \mathbf{B} \rangle$ of the wave breaking momentum flux, since it is responsible for driving the mean longshore current $\langle v \rangle$. The addition of a mean longshore current to the flow field does not change the wavefield, since the longshore velocity v only appears in the wave energy equation (17) as

$$\frac{\partial v}{\partial y}\langle E \rangle = \frac{\partial \widetilde{v}}{\partial y}\langle E \rangle.$$

However, the longshore current does affect the cross-shore current u through the advection term $v\partial u/\partial y$ in (6), and, in this way, modifies the wavefield indirectly. At 1°, $\nabla^{\perp} \cdot \widetilde{\mathbf{B}}$ is essentially equivalent to its WEC+CEW value at 0° (see Figure 4b), while at 6°, $\nabla^{\perp} \cdot \mathbf{B}$ is nearly identical to its WEC-only value at 0° (Figure 4a). Thus, as the angle of incidence θ of the waves increases, the CEW decrease in magnitude.

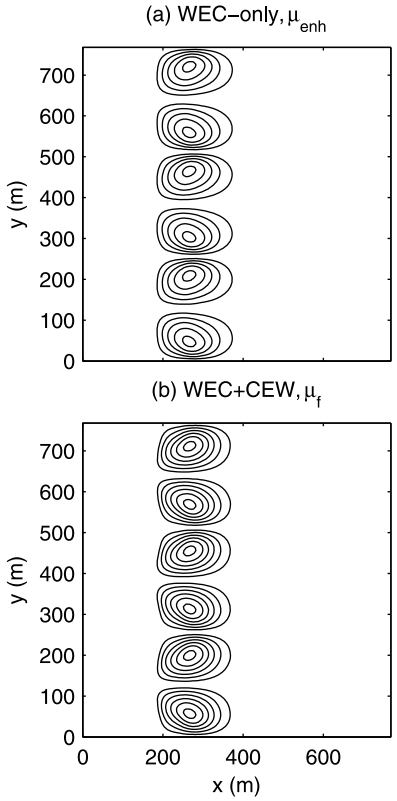

Figure 10. Comparison of rip current velocity of (a) the WEC-only model with the enhanced bottom friction $\mu_{\text{enh}} = 0.0065$ m s^{-1} and (b) the WEC+CEW model with $\mu_f = 0.002$ m s^{-1}. The streamlines are plotted at 3 m^3 s^{-1} intervals of ψ. The ratio of this number to the spacing between adjacent contours is approximately $|\nabla\psi| = |h(\mathrm{u} + \mathbf{u}^{\mathrm{St}})|$. The current speed is thus inversely proportional to the product of the depth and the contour spacing.

[42] This decrease occurs because the streamlines of the rip current tilt to align opposite to the incoming angle of the waves (Figure 15); the longshore current generated by the incoming waves causes the feeder flow of the rips to be stronger in the direction of the waves, which then causes the rips to be directed away from the direction the waves. As the angle increases, the circulation cells characteristic of rip currents in Figures 15a and 15d give way to unbounded streamlines aligned with the alongshore direction in Figures 15c and 15f. The gradual aligning of the streamlines with the longshore direction diminishes the magnitude of $\partial\psi/\partial y$, which causes the cross-shore velocity u and its longshore derivative $\partial u/\partial y$ to decrease in magnitude as well, thus decreasing the magnitude of the CEW.

[43] If the perturbation to the longshore bar has a magnitude $\varepsilon = 0.1$, then for waves with an angle of incidence greater than approximately 6°, the resulting currents resemble the longshore current with an $O(\varepsilon)$ perturbation. We do not consider this flow here, since it is covered extensively in the literature on the longshore current [*Allen et al.*, 1996]. In particular, *Uchiyama et al.* [2009] apply the VF formalism to the dynamics of longshore currents.

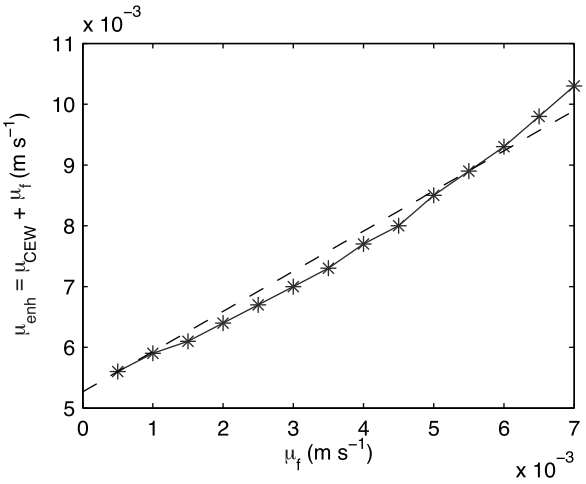

Figure 11. Enhanced bottom friction μ_{enh} (solid) as a function of true bottom friction μ_f, and a linear least squares fit (dashed). The slope of the fitted line is approximately 0.66, and its y intercept is $\mu_{\text{enh}} \approx 0.0053$ m s^{-1}.

3.8. Bottom Drag

[44] In this section we consider three bottom drag parameterizations: two of which are nonlinear and take into account both the current and wave velocities and Rayleigh bottom friction, which depends linearly on the current velocity.

[45] In the presence of waves and currents, the most common model for the bottom drag on the current [*Sleath*, 1984] is

$$\boldsymbol{\tau}_b = \rho c_f \overline{|\mathbf{u}^{\mathrm{tot}}|\mathbf{u}^{\mathrm{tot}}},$$

where $\mathbf{u}^{\mathrm{tot}}$ is the total velocity due to waves and currents, and the overline denotes averaging over several wave periods.

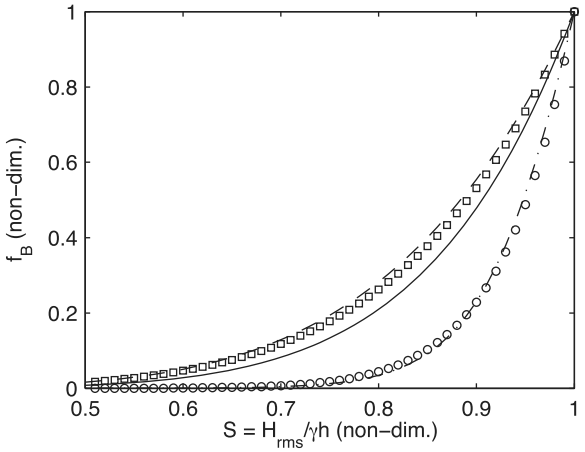

Figure 12. Dependence of the TG83a (solid), TG83b (dashed), and CT93 (dot-dashed) wave breaking parameterizations on the coefficient of wave energy saturation $S = H_{\mathrm{rms}}/\gamma h$. For comparison, S^6 (squares) and S^{14} (circles) are also plotted. The functions have been normalized so that $f_B(1) = 1$ for every parameterization.

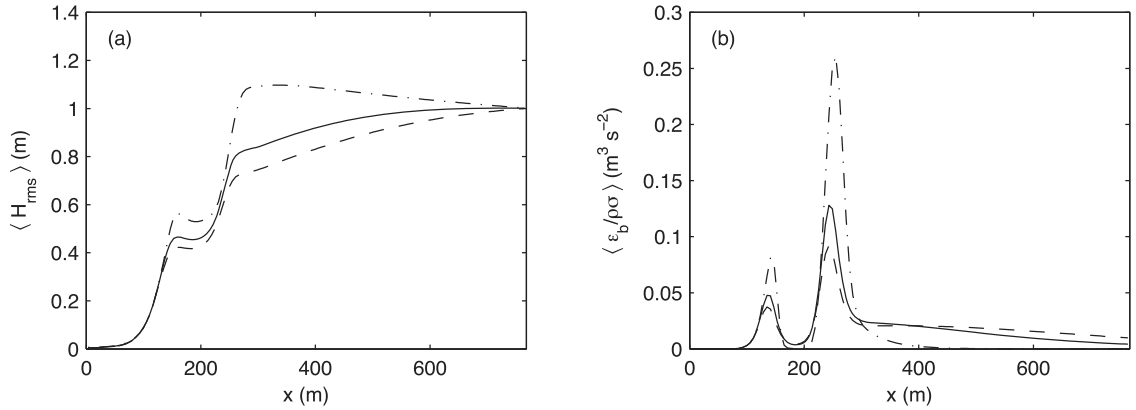

Figure 13. Alongshore means of (a) wave height and (b) wave breaking for three different wave breaking parameterizations: TG83a (solid), TG83b (dashed), and CT93 (dot-dashed).

There are many choices for the bottom friction coefficient c_f. Two examples are

$$c_f = \left(\frac{\kappa}{1+\ln(z_0/h)}\right)^2 \quad \text{or} \quad c_f = 0.01525\left(\frac{k_s}{H}\right)^{1/3}.$$

The first is derived by *Soulsby* [1997] as a best possible fit for a number of experimental results. The second is the Manning-Strickler law. Here $\kappa = 0.4$ is the von Kármán constant, and z_0 is the bed roughness length. We use $z_0 = d_{50}/12 = 10^{-3}$ m and take the apparent roughness length (or, Nikuradse roughness length) as $k_s = 0.0125$ m. In general, the two forms for c_f are quite similar, so we restrict our attention to the Manning-Strickler law.

[46] The bottom friction parameterization of *Soulsby* [1995] represents the combined influence of waves and currents as a function of the individual current $\boldsymbol{\tau}_c$ and wave $\boldsymbol{\tau}_w$ shear stresses. It is

$$\boldsymbol{\tau}_b = \boldsymbol{\tau}_c\left[1 + 1.2\left(\frac{|\boldsymbol{\tau}_w|}{|\boldsymbol{\tau}_c| + |\boldsymbol{\tau}_w|}\right)^{3.2}\right]. \tag{24}$$

[47] The individual shear stresses are defined as

$$\boldsymbol{\tau}_c = \rho c_f |\mathbf{u}|\mathbf{u}, \quad \text{and} \quad \boldsymbol{\tau}_w = \frac{1}{2}\rho f_w \left(u_b^{wv}\right)^2, \tag{25}$$

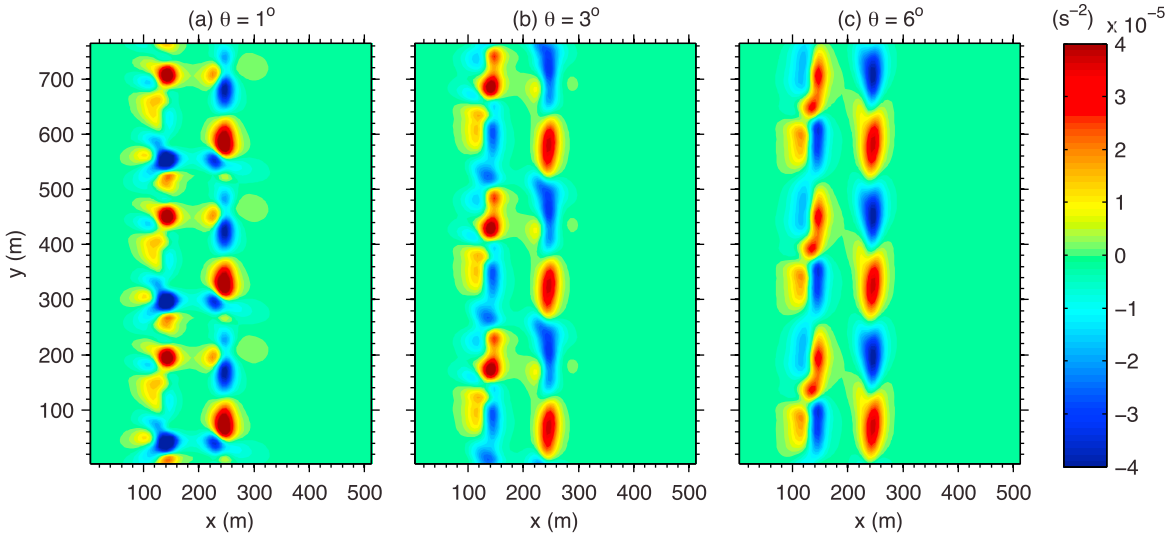

Figure 14. Longshore fluctuations of the forcing of vorticity $\nabla^\perp \cdot \widetilde{\mathbf{B}}$ for the WEC+CEW model type and an angle of incidence (a) $\theta = 1°$, (b) $\theta = 3°$, and (c) $\theta = 6°$. Compare Figure 14a with Figure 4b and Figure 14c with Figure 4a. The alongshore mean $\nabla^\perp \cdot \langle \mathbf{B} \rangle$ (not pictured) is the forcing for the longshore current vorticity and increases with θ.

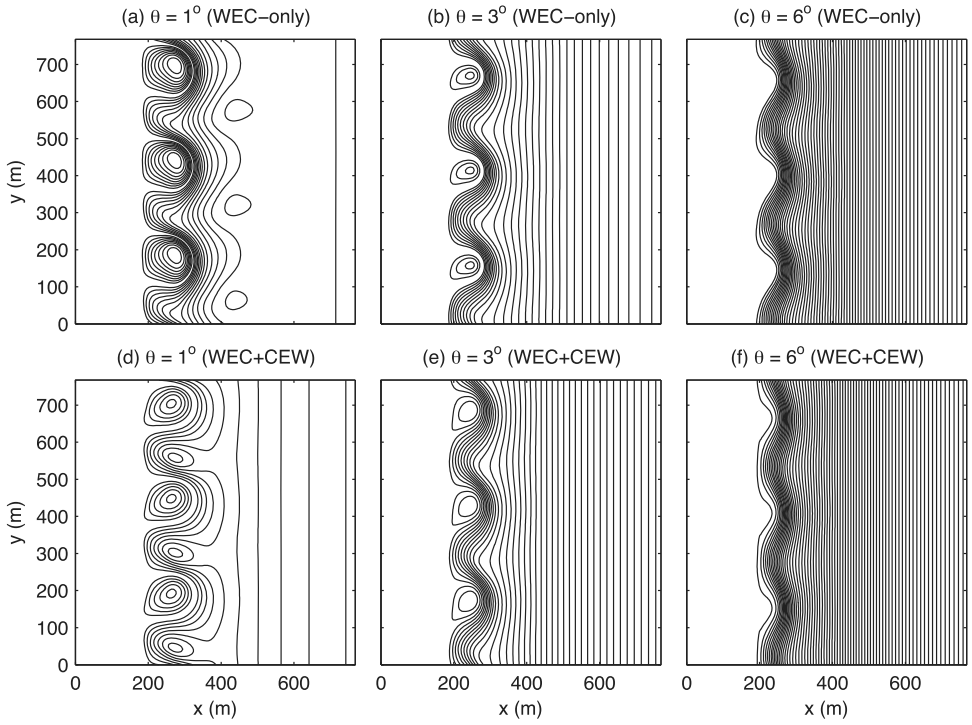

Figure 15. Dependence of the current streamlines on the angle of incidence of the waves.

where f_w is an empirical wave friction factor

$$f_w = 1.39\left(\frac{u_b^{wv}}{\sigma z_0}\right)^{-0.52}$$

and u_b^{wv} is the wave orbital bottom velocity. For a monochromatic wave, it is

$$u_b^{wv} = \frac{\sigma A}{\sinh(kH)},$$

which is the velocity such that for the linear wave theory, the velocity at the bottom $z = -H$ would be

$$u_b^{wv}\cos(\mathbf{k}\cdot\tilde{\mathbf{x}} - \sigma\tilde{t}),$$

where $\tilde{\mathbf{x}}$ and $\tilde{t}$ are the spatiotemporal coordinates of the wave variables, i.e., the variables $\mathbf{x}$ and t before the wave averaging.

[48] A second nonlinear parameterization of bottom stress that we consider was proposed by *Feddersen et al.* [2000]

$$\boldsymbol{\tau}_b = \rho c_f\left[(1.16)^2 + \left(\frac{|\mathbf{u}|}{u_{rms}^{wv}}\right)^2\right]^{1/2} u_{rms}^{wv}\mathbf{u},$$

where u_{rms}^{wv} is the root-mean-square wave orbital velocity, such that when the waves have a single spectral peak

$$u_{rms}^{wv} = \frac{1}{\sqrt{2}}u_b^{wv}.$$

[49] When the angle of incidence of the waves is almost normal, and the currents are weak compared to the waves, we use the approximation

$$\overline{|\mathbf{u}^{tot}|\mathbf{u}^{tot}} \approx \frac{2}{\pi}u_b^{wv}\mathbf{u}.$$

In reality, there is an asymmetry between the cross-shore and longshore components of this frictional term, with the factor of the cross-shore component being $4/\pi$. Following *Dodd* [1994] and *Özkan-Haller and Kirby* [1999] we use the symmetric form instead, as it tends to give similar results, and in practice the uncertainty in the bottom friction coefficient makes this simplification even more germane. The longshore mean of the factor $(2/\pi)\,u_b^{wv}$, depicted in Figure 16, varies over space and time. A common approximation is to take its steady state WEC-only value averaged over both spatial directions (dashed line). We may then write

$$\boldsymbol{\tau}_b = \rho\mu_f\mathbf{u},$$

where we have defined the *linear* bottom friction coefficient as

$$\mu_f = \frac{2}{\pi}\frac{1}{L}\int_0^L \langle c_f u_b^{wv}\rangle\, dx,$$

where, as before, $\langle\cdot\rangle$ is the longshore mean and L is the domain length in the cross-shore direction. This is the Rayleigh bottom friction model. For the WEC-only model,

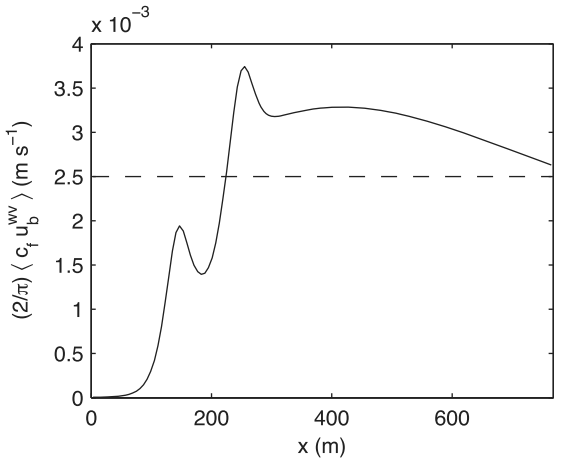

Figure 16. The alongshore mean of the factor $(2/\pi)\, c_f\, u_b^{wv}$ for the Manning-Strickler law (solid) and its cross-shore average (dashed). The *Soulsby* [1997] bottom drag coefficient is not pictured.

the Soulsby and Feddersen results are nearly identical to the results for a constant bottom friction of $\mu_f = 0.002$ m s^{-1} (see Figures 17a–17c). We see in fact that the approximation of μ_f in Figure 16 slightly overestimates the bottom friction, since the most important values of the friction are in the neighborhood of the trough shoreward of the bar. The negative feedback loop on the currents formed by adding CEW makes the WEC+CEW model results even less dependent on the particular bottom drag law (Figures 17d–17f). Both *Özkan-Haller and Kirby* [1999] and *Thornton and Guza* [1986] suggest that this agreement holds even in the extreme case when the currents are strong and a nonlinear model is expected to be more appropriate.

4. Conclusions

[50] We have shown that rip currents reduce the flux of momentum from waves to currents due to wave breaking. The bending of wave rays by currents and current flux forces wave energy into the channels of the longshore bar. This reduces the longshore variation of the flux of momentum due to wave breaking. We detailed precisely the calculation of the change in the wavefield due to wave ray bending and due to the current flux of wave energy. This calculation gives the added geophysical insight that the ratio of these two forces scales as the square of the ratio of the typical length to width of the rip currents. This confirms the finding of YS03 that neglecting the wave ray bending in rip current calculations is not appropriate, since it is the dominant current effect on the wave energy. We then showed that the vortex force is equivalent to the cross-shore flux of vorticity by the mean Stokes drift, and in the absence of other WEC, it is unchanged by CEW. The CEW form a negative feedback loop on the currents. We defined a parameter μ_{CEW} that measures the best fit of this dissipative force with linear bottom friction. We found that the enhanced friction, the sum of this fictitious friction and the true bottom friction, had a minimum greater than 0.005 m s^{-1}. For the physical scenario we considered numerically, the WEC-only model is

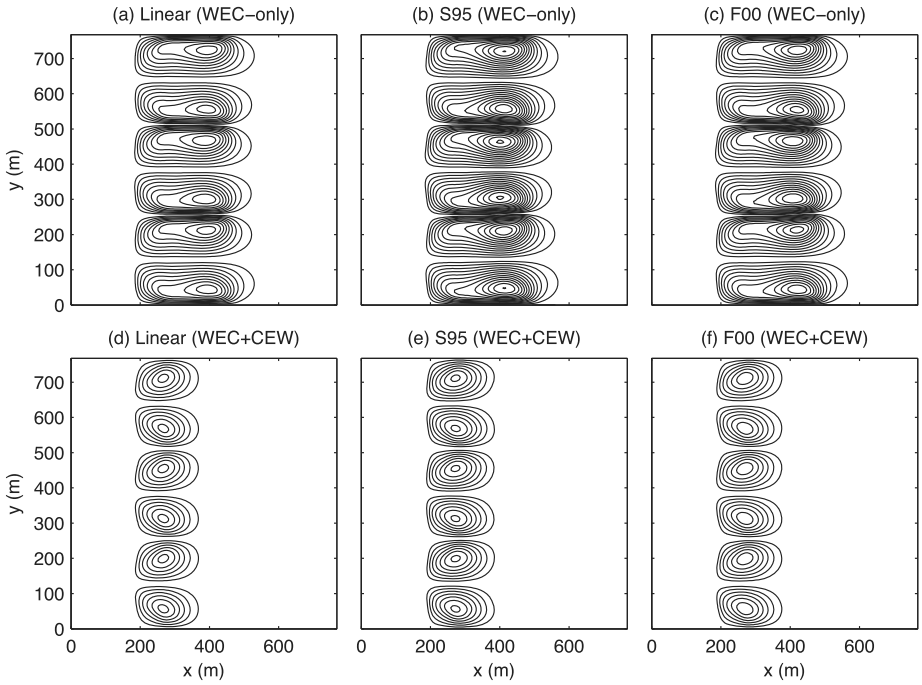

Figure 17. Current streamlines at (a–c) $t = 50$ min for the WEC-only model and (d–f) steady state values for the WEC+CEW model, for the linear bottom friction with $\mu_f = 0.002$ m s^{-1} (Figures 17a and 17d), the nonlinear model of *Soulsby* [1995] (S95, Figures 17b and 17e), and the nonlinear model of *Feddersen et al.* [2000] (F00, Figures 17c and 17f).

stable at this value of the bottom friction. As the angle of incidence of the waves increases, the CEW decrease in magnitude. For an $O(0.1)$ perturbation to the longshore bar, the CEW are negligible when the angle of incidence exceeds 6°. These results hold for any wave breaking parameterization whose dependence on the coefficient of wave energy saturation $S = H_{\rm rms}/\gamma h$ is well approximated by a power law. Based on our analysis, this property is generic to breaking parameterizations for narrow-banded swell. The exponent of this power law determines both the strength and stability of the predicted rips.

Appendix A: Equivalence of the VF and RS Formalisms

[51] We consider the two RS model types from YS03: "interaction," where the wave variables are dynamic, and "no interaction," where the wave variables are the steady state values computed without CEW. Both model types use the current equations

$$\frac{\partial \mathbf{U}}{\partial t} + \mathbf{U}\cdot\nabla\mathbf{U} + \frac{1}{\rho}\nabla\Phi = \boldsymbol{\tau} - \mathbf{D}^{\mathbf{L}}, \tag{A1}$$

$$\nabla\cdot(h\mathbf{U}) = 0, \tag{A2}$$

and the velocity field $\mathbf{U}$ is used in the wave equations (3) and (5). The WEC τ is the divergence of the radiation stress tensor S_{ij}. It is defined as

$$\tau_i = -\frac{1}{\rho h}\left(\frac{\partial S_{i1}}{\partial x} + \frac{\partial S_{i2}}{\partial y}\right), \qquad i = 1,2. \tag{A3}$$

where the radiation stress tensor is

$$S_{ij} = \frac{\mathcal{A}\sigma}{2}\left[\frac{2C_g}{c}\frac{k_i k_j}{k^2} + \left(\frac{2C_g}{c} - 1\right)\delta_{ij}\right], \tag{A4}$$

δ_{ij} is the Kronecker delta function, $C_g = |\mathbf{C_g}|$, and $c = \sigma/k$ is the phase velocity. Upon substitution we find

$$\tau = -\frac{1}{\rho h}\left[\mathbf{k}\nabla\cdot(\mathbf{C_g}\mathcal{A}) + \mathcal{A}(\mathbf{C_g}\cdot\nabla\mathbf{k}) + \nabla\left(\frac{\mathcal{A}\sigma kh}{\sinh 2kh}\right)\right].$$

The bottom drag is

$$\mathbf{D}^{L} = \mu_f\frac{\mathbf{U}}{h},$$

where we have used the "L" to denote it's dependence on the Lagrangian current $\mathbf{U}$, and not the Eulerian current $\mathbf{u}$.

[52] Now suppose $\mathbf{U} = \mathbf{u} + \mathbf{u}^{\rm St}$, so that (A2) is equivalent to (7). Suppose further that the vorticity $\chi^{\rm St} = \nabla^{\perp}\cdot\mathbf{u}^{\rm St}$ is $O(\nu)$ compared to the current vorticity χ, where ν is a small parameter. Under this assumption, the curl of (A1) is

$$\frac{\partial\chi}{\partial t} + \nabla\cdot\left[(\mathbf{u}+\mathbf{u}^{\rm St})\chi\right] = \nabla^{\perp}\cdot(\boldsymbol{\tau} + \mathbf{D}^{\mathbf{L}}).$$

The parameter $\nu = \mu_f/(\sigma h)$ is typically $O(10^{-2})$.

[53] The Lagrangian bottom drag does not change the dissipation of the current since

$$\begin{aligned}\nabla^{\perp}\cdot\mathbf{D}^{L} &= \nabla^{\perp}\cdot\left[\frac{\mu_f}{h}(\mathbf{u}+\mathbf{u}^{\rm St})\right]\\ &= \frac{\mu_f}{h}\left[\nabla^{\perp}\cdot\mathbf{U} - \frac{1}{h}(\mathbf{u}+\mathbf{u}^{\rm St})\cdot\nabla^{\perp}h\right] + O(\nu).\end{aligned}$$

Using the shallow water approximation of (8) we find

$$\frac{1}{h}\mathbf{u}^{\rm St}\cdot\nabla^{\perp}h = \frac{1}{h}\frac{A^2\sigma}{2(kh)^2}\mathbf{k}\cdot\nabla^{\perp}h = -\left(\frac{A^2\sigma}{2h^2}\right)\frac{\mathbf{k}^{\perp}}{k}\cdot\frac{\nabla h}{kh},$$

where

$$\left|\frac{A^2\sigma}{2h^2}\frac{\mathbf{k}^{\perp}}{k}\right| = \frac{1}{2}O\left(\sigma\left(\frac{A}{h}\right)^2\right) \le \frac{1}{8}\sigma\gamma^2 \approx 0.01,$$

and the term $|\nabla h/kh|$ is small by assumption, as it measures the variation of the bottom topography [*Mei*, 1989]. Hence, the differences between the Lagrangian and Eulerian bottom drags are lower order.

[54] Using equations (3) and (5), we find that the divergence of the radiation stress tensor is

$$\boldsymbol{\tau} = \mathbf{B} + \nabla\varphi,$$

where φ is a function of the wave variables. When there is no interaction,

$$\varphi = g\hat{\zeta} = -g\frac{A^2k}{2\sinh 2kh},$$

where $\hat{\zeta}$ is the quasi-static response of the waves. When there is interaction,

$$\varphi = g\hat{\zeta} - \frac{1}{2}|\mathbf{u}^{\rm St}|^2.$$

Equations (A1) and (A2) are thus equivalent to equations (6) and (7) with a change in the pressure term, which the flow velocity is independent of, because we neglect wave set up.

[55] Finally, for the interaction equations, we must show that using the Lagrangian velocity $\mathbf{U}$ rather than the Eulerian velocity $\mathbf{u}$ does not affect the wave variables. This follows since the magnitude of the group velocity dominates the magnitude of the Stokes drift, i.e.,

$$\frac{u_i^{\rm St}}{C_{g_i}} = \frac{1}{8}\left(\frac{H_{\rm rms}}{h}\right)^2 \le \frac{1}{8}\gamma^2 \approx 0.02, \qquad i = 1,2.$$

Thus, YS03's interaction model is equivalent to our WEC+CEW model, and their no interaction model equivalent to our WEC-only model.

[56] **Acknowledgments.** This research is supported by the National Science Foundation under grant DMS-0723757 and the Office of Naval Research under grant N00014-04-1-0166. J.M.R. acknowledges the Institute for Mathematics and its applications, where part of this work was performed.

References

Allen, J. S., P. A. Newberger, and R. A. Holman (1996), Nonlinear shear instabilities of alongshore currents on plane beaches, *J. Fluid Mech.*, *310*, 181–213.

Bowen, A. J. (1969), Rip currents: 1. Theoretical investigations, *J. Geophys. Res.*, *74*(23), 5467–5478.
Bowen, A. J., and D. L. Inman (1969), Rip currents: 2. Laboratory and field observations, *J. Geophys. Res.*, *74*(23), 5479–5490.
Church, J. C., and E. B. Thornton (1993), Effects of breaking wave induced turbulence within a longshore current model, *Coastal Eng.*, *20*, 1–28.
Craik, A. D. D., and S. Leibovich (1976), A rational model for Langmuir circulations, *J. Fluid Mech.*, *73*, 401–426.
Dalrymple, R. A., and C. T. Lozano (1978), Wave-current interaction models for rip currents, *J. Geophys. Res.*, *83*(C12), 6063–6071.
Dodd, N. (1994), On the destabilization of a longshore current on a plane beach: Bottom shear stress, critical conditions, and onset of instability, *J. Geophys. Res.*, *99*(C1), 811–824.
Falqués, A., A. Montoto, and D. Vila (1999), A note on hydrodynamic instabilities and horizontal circulation in the surf zone, *J. Geophys. Res.*, *104*(C9), 20,605–20,615.
Feddersen, F., R. Guza, S. Elgar, and T. Herbers (2000), Velocity moments in alongshore bottom stress parameterizations, *J. Geophys. Res.*, *105*, 8673–8686.
Haas, K. A., I. A. Svendsen, M. C. Haller, and Q. Zhao (2003), Quasi-three-dimensional modeling of rip current systems, *J. Geophys. Res.*, *108*(C7), 3217, doi:10.1029/2002JC001355.
Haller, M. C., and R. A. Dalrymple (2001), Rip current instabilities, *J. Fluid Mech.*, *433*, 161–192.
Hasan, H., N. Dodd, and R. Garnier (2009), Stabilizing effect of random waves on rip currents, *J. Geophys. Res.*, *114*, C07010, doi:10.1029/2008JC005031.
Hasselmann, K. (1971), On the mass and momentum transfer between short gravity waves and larger-scale motions, *J. Fluid Mech.*, *50*, 189–201.
Kennedy, A. B., and Y. Zhang (2008), The stability of wave-driven rip current circulation, *J. Geophys. Res.*, *113*, C03031, doi:10.1029/2006JC003814.
Lane, E. M., J. M. Restrepo, and J. C. McWilliams (2007), Wave-current interaction: A comparison of radiation-stress and vortex-force representations, *J. Phys. Oceanogr.*, *37*, 1122–1141.
LeBlond, P. H., and C. L. Tang (1974), On energy coupling between waves and rip currents, *J. Geophys. Res.*, *79*(6), 811–816.
LeMehaute, B. (1962), On non-saturated breakers and the wave run-up, paper presented at 8th International Conference on Coastal Engineering, Am. Soc.of Civ. Eng., Mexico City.
LeVeque, R. (2002), *Finite Volume Methods for Hyperbolic Problems*, Cambridge Univ. Press, Cambridge, U. K.
Lippmann, T. C., T. H. C. Herbers, and E. B. Thornton (1999), Gravity and shear wave contributions to nearshore infragravity motions, *J. Phys. Oceanogr.*, *29*, 231–239.
Longuet-Higgins, M. S., and R. W. Stewart (1960), Changes in the form of short gravity waves on long waves and tidal currents, *J. Fluid Mech.*, *8*, 565–583, doi:10.1017/S0022112060000803.
Longuet-Higgins, M. S., and R. W. Stewart (1961), The changes in amplitude of short gravity waves on steady non-uniform currents, *J. Fluid Mech.*, *10*, 529–549, doi:10.1017/S0022112061000342.
Longuet-Higgins, M. S., and R. W. Stewart (1962), Radiation stress and mass transport in gravity waves, with application to "surf beats", *J. Fluid Mech.*, *13*, 481–504.
Longuet-Higgins, M. S., and R. W. Stewart (1964), Radiation stresses in water waves: A physical discussion, with applications, *Deep Sea Res.*, *11*, 529–562.
McKenzie, P. (1958), Rip current system, *J. Geol.*, *66*, 103–113.
McWilliams, J. C., J. M. Restrepo, and E. M. Lane (2004), An asymptotic theory for the interaction of waves and currents in coastal waters, *J. Fluid Mech.*, *511*, 135–178.
Mei, C. C. (1989), *The Applied Dynamics of Ocean Surface Waves*, 740 pp., World Sci., Singapore.
Noda, E. K. (1974), Wave-induced nearshore circulation, *J. Geophys. Res.*, *79*(27), 4097–4106.
Özkan-Haller, H. T., and J. T. Kirby (1999), Nonlinear evolution of shear instabilities of the longshore current: A comparison of observations and computations, *J. Geophys. Res.*, *104*(C11), 25,953–25,984.
Roelvink, J. (1993), Dissipation in random wave groups incident on a beach, *Coastal Eng.*, *19*, 127–150.
Shepard, F. P. (1936), Undertow, rip tide or "rip current", *Science*, *84*(2173), 181–182.
Shepard, F. P., and D. L. Inman (1950), Nearshore circulation related to bottom topography and wave refraction, *Eos Trans. AGU*, *31*(4), 555–565.
Shepard, F. P., K. O. Emery, and E. C. L. Fond (1941), Rip currents: A process of geological importance, *J. Geol.*, *49*, 337–369.
Sleath, J. F. A. (1984), *Sea Bed Mechanics*, John Wiley, New York.
Sonu, C. J. (1972), Field observation of nearshore circulation and meandering currents, *J. Geophys. Res.*, *77*(18), 3232–3247.
Soulsby, R. (1997), *Dynamics of marine sands*, Thomas Telford, London.
Soulsby, R. L. (1995), Bed shear-stresses due to combined waves and currents, in *Advances in Coastal Morphodynamics*, edited by M. J. F. Stive et al., pp. 4-20–4-23, Delft Hydraulics, Delft, Netherlands.
Thornton, E. B., and R. T. Guza (1983), Transformation of wave height distribution, *J. Geophys. Res.*, *88*(C10), 5929–5938.
Thornton, E. B., and R. T. Guza (1986), Surf zone longshore currents and random waves: Field data and models, *J. Phys. Oceanogr.*, *16*, 1165–1178.
Uchiyama, Y., J. C. McWilliams, and J. M. Restrepo (2009), Wave-current interaction in nearshore shear instability analyzed with a vortex-force formalism, *J. Geophys. Res.*, *114*, C06021, doi:10.1029/2008JC005135.
Yu, J. (2006), On the instability leading to rip currents due to wave-current interaction, *J. Fluid Mech.*, *549*, 403–428.
Yu, J., and D. N. Slinn (2003), Effects of wave-current interaction on rip currents, *J. Geophys. Res.*, *108*(C3), 3088, doi:10.1029/2001JC001105.

E. M. Lane, Hydrodynamics Group, National Institute for Water and Atmospheric Research, 10 Kyle St., Riccarton, Christchurch 8011, New Zealand.
J. C. McWilliams and Y. Uchiyama, Institute of Geophysics and Planetary Physics, University of California, Los Angeles, 3845 Slichter Hall, 603 Charles E. Young Dr., E., Los Angeles, CA 90065-1567, USA.
J. M. Restrepo and B. Weir, Department of Mathematics, University of Arizona, Tucson, AZ 85721-0089, USA. (bweir@math.arizona.edu)